
This is an electronic reprint of the original article.
This reprint may differ from the original in pagination and typographic detail.

Ketola, Annika E.; Xiang, Wenchao; Hjelt, Tuomo; Pajari, Heikki; Tammelin, Tekla; Rojas, Orlando J.; Ketoja, Jukka A.

Bubble Attachment to Cellulose and Silica Surfaces of Varied Surface Energies : Wetting Transition and Implications in Foam Forming

Published in:
Langmuir

DOI:
[10.1021/acs.langmuir.0c00682](https://doi.org/10.1021/acs.langmuir.0c00682)

Published: 07/07/2020

Document Version
Publisher's PDF, also known as Version of record

Published under the following license:
CC BY

Please cite the original version:
Ketola, A. E., Xiang, W., Hjelt, T., Pajari, H., Tammelin, T., Rojas, O. J., & Ketoja, J. A. (2020). Bubble Attachment to Cellulose and Silica Surfaces of Varied Surface Energies : Wetting Transition and Implications in Foam Forming. *Langmuir*, 36(26), 7296-7308. <https://doi.org/10.1021/acs.langmuir.0c00682>

This material is protected by copyright and other intellectual property rights, and duplication or sale of all or part of any of the repository collections is not permitted, except that material may be duplicated by you for your research use or educational purposes in electronic or print form. You must obtain permission for any other use. Electronic or print copies may not be offered, whether for sale or otherwise to anyone who is not an authorised user.

Bubble Attachment to Cellulose and Silica Surfaces of Varied Surface Energies: Wetting Transition and Implications in Foam Forming

Annika E. Ketola, Wenchao Xiang, Tuomo Hjelt, Heikki Pajari, Tekla Tammelin, Orlando J. Rojas, and Jukka A. Ketoja*



Cite This: *Langmuir* 2020, 36, 7296–7308



Read Online

ACCESS |



Metrics & More

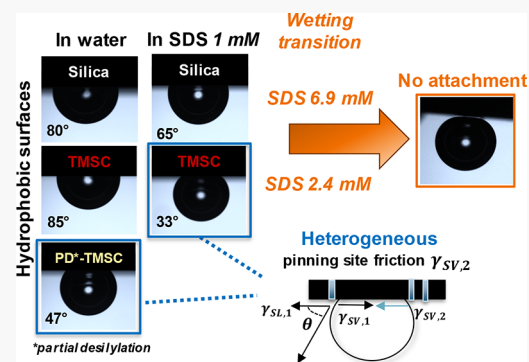


Article Recommendations



Supporting Information

ABSTRACT: To better understand the complex system of wet foams in the presence of cellulosic fibers, we investigate bubble–surface interactions by following the effects of surface hydrophobicity and surface tension on the contact angle of captive bubbles. Bubbles are brought into contact with model silica and cellulose surfaces immersed in solutions of a foaming surfactant (sodium dodecyl sulfate) of different concentrations. It is observed that bubble attachment is controlled by surface wetting, but a significant scatter in the behavior occurs near the transition from partial to complete wetting. For chemically homogeneous silica surfaces, this transition during bubble attachment is described by the balance between the energy changes of the immersed surface and the frictional surface tension of the moving three-phase contact line. The situation is more complex with chemically heterogeneous, hydrophobic trimethylsilyl cellulose (TMSC). TMSC regeneration, which yields hydrophilic cellulose, causes a dramatic drop in the bubble contact angle. Moreover, a high interfacial tension is required to overcome the friction caused by microscopic (hydrophilic) pinning sites of the three-phase contact line during bubble attachment. A simple theoretical framework is introduced to explain our experimental observations.



INTRODUCTION

Cellulosic microfibrils are versatile biobased materials possessing high strength and relatively low density. They are the reinforcing structural component of plant cell walls, making cellulose the most abundant biomolecule in the biosphere. The use of cellulose fibers in materials such as paper and board makes them easily recyclable and biodegradable. Demand for greener materials is growing fast, and cellulose could be one potential option. Cellulose fibers could be applied, for example, in high-performance materials and products such as soft packaging, air filters, and substrates for biocatalytic conversion.

Foam forming^{1–3} of fibers into paper webs and textile fabrics is a relatively new and versatile modification of papermaking technology. It can be used to produce materials from thick, porous, and lightweight structures to thin fabrics and stratified materials (Figure 1b).^{4–6} In foam forming, fibers are mixed with water and surfactants, and shear forces are applied to create wet foam (Figure 1a). The wet foam is guided onto a wire, and the liquid in the foam is removed by vacuum drainage and drying with heat, leaving a self-standing dry fiber structure. As this technology is relatively new, research has focused on a better understanding of the fundamentals of the wet fiber foam system (drainage rate, bubble size distribution, coarsening rate)^{7–10} and its effects on dry material properties.^{11–14}

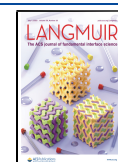
Previous studies have shown that even though bubbles do not form clear three-phase contact with fiber surfaces, they are often found weakly attached to the fibers (Figure 1c).^{9,15,16} Bubbles and fibers both carry a negative charge in aqueous solutions,^{17–22} meaning that the net interaction should be repulsive. Flotation deinking studies have shown that the removal of fibers with froth is mostly dominated by physical entrainment of fibers,^{23–25} and actual bubble attachment to fibers rarely takes place. However, many of the results have been controversial, and the contributions of different forces in bubble–fiber interactions are still unclear.

Bubble attachment and detachment on (from) solid mineral particles are important for the recovery of collected minerals in froth flotation,^{26,27} and the mechanisms underlying bubble–particle interactions have been studied comprehensively.^{28–35} The stability of the wetting film between bubbles and particles dictates whether the bubble forms a three-phase contact with

Received: March 11, 2020

Revised: June 6, 2020

Published: June 8, 2020



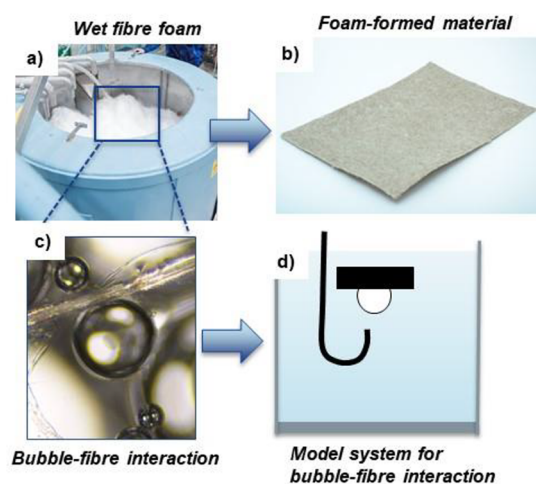


Figure 1. (a) Fiber-foam mixing tank of the foam forming process. (b) Thin foam-formed fiber fabric (mixture of natural and textile fibers). (c) Light microscopy image of the interaction between bubbles and pine fiber in wet foam obtained with SDS surfactant. (d) Captive bubble measurement system.

the surface. This stability depends greatly on the particle hydrophobicity, charge, and surface tension.^{29,36} In froth flotation, also the kinetics of bubble collision with mineral particles is highly important and is usually studied using simple bubble–particle collision systems.^{26,37,38} The collision kinetics has been studied for several mineral surfaces, such as mica, quartz, Teflon, graphite, and molybdenite.^{26,36,37,39–41} However, there are few studies in which bubble interaction with biopolymers has been addressed.^{38,40,41}

In general, bubbles readily form a three-phase contact with hydrophobic particles but repel hydrophilic particles, and adsorption of surfactants and polymers can fully reverse this interaction.^{26,41} Therefore, it is also important to study the connection between the bubble contact angle and surface tension of the system and model these phenomena. This can be done using the well-defined theory of wetting and spreading.⁴² In the out-of-equilibrium situation, the dynamic contact angle generally depends on physical scale due to large-scale hydrodynamics and microscopic molecular effects.

Moreover, impurities, surface roughness, or chemical surface heterogeneity may prevent reaching of the equilibrium state.⁴²

Danov et al.⁴³ studied the adhesion of bubbles on solid surfaces by capillary meniscus dynamometry. They measured the maximal pulling force required to release a bubble from a surface and described it in terms of attractive transversal tension and repulsive disjoining pressure. We apply a similar captive bubble method^{44–46} (Figure 1d) to smooth thin films of regenerated cellulose and modified silica of different hydrophobicity spin-coated on silica substrates. Regenerated cellulose is a so-called “man-made” cellulose that is produced by converting natural cellulose into a soluble derivative (here trimethylsilyl cellulose, TMSC) and then regenerating it back to cellulose.^{47,48} Model surfaces were immersed in anionic surfactant (sodium dodecyl sulfate, SDS) solutions of different concentrations. Our choice to use SDS stems from the fact that it is a typical reference in the literature, but most importantly, it is commonly used for foam forming with wood fibers. SDS adsorption on the model surfaces and its possible effect on surface wetting were determined using the quartz crystal microbalance with dissipation (QCM-D) technique. The results are interpreted in terms of calculated changes in interfacial energy during bubble attachment. This study, which simplifies the bubble–surface systems, sets a basis for more complex, future exploration of the connections between the properties of wet foams and dry fiber networks.

EXPERIMENTAL SECTION

An overview of the experimental setup, including the prepared model surfaces, test solutions, and measurement methods, is shown in Table 1.

Materials. All reagents used in the experiments were analytical grade. Anionic surfactant sodium dodecyl sulfate (SDS, purity $\geq 99\%$) was purchased from Sigma-Aldrich (Germany) and was used without further purification. Sodium hydroxide (NaOH) and sodium chloride (NaCl) were purchased from Merck (Germany). Ethanol (Etax, AA-grade) was purchased from Altia Oyj (Finland), chlorotrimethylsilane (CTMS) from Sigma-Aldrich (Germany), xylene from Prolabo (France), and toluene from VWR International (France). Diiodomethane (DIM) was obtained from Sigma-Aldrich (India), formamide from J. T. Baker (Holland), and ethylene glycol from Fluka. Water used in the experiments was Milli-Q purified.

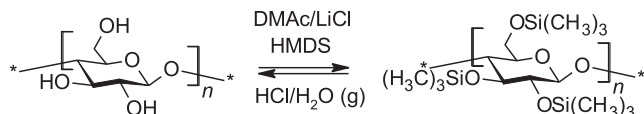
Table 1. Experimental Setup with Used Test Solutions, Measurements Conducted, and Model Surface Characteristics, Including Drop Contact Angle (θ_D), Root-Mean-Square (RMS) Roughness, and Surface Free Energy (γ_{SV}) with Dispersive (γ_d) and Polar (γ_p) Components (Based on the OWRK/Fowkes Method)^a

	surface	surface code	θ_D	RMS ^b (nm)	surface free energy (mN/m)		
					γ_{SV}	γ_d	γ_p
hydrophilic surfaces	hydrophilic silica	Si–OH	$5^\circ \pm 4^\circ$	0.4	64.6	34.1	30.5
	cellulose	Si–CellOH	$25^\circ \pm 5^\circ$	1.5	60.2	39.3	21
hydrophobic surfaces	hydrophobic silica	Si–CH ₃	$100^\circ \pm 7^\circ$	3.4	22	20.3	1.7
	TMSC	Si–TMSC	$93^\circ \pm 1^\circ$	4.4	21.4 ^c	21.4 ^c	0 ^c
test solutions	SDS at concentrations of 0–8.3 mM						
	SDS in 0.01 M NaCl at concentrations of 0–8.3 mM						
measurements	captive bubble						
	QCM-D						
surface characterization	sessile drop						
	surface free energy						
	AFM						

^aTMSC stands for trimethylsilyl cellulose and CellOH for cellulose. ^bRMS values were analyzed from AFM images shown in Figure S3 (area $5 \times 5 \mu\text{m}^2$). ^cSurface free energy of pure Si–TMSC was not measured, but a value of 21.4 mN/m has been reported in the literature.⁴⁹

Trimethylsilyl Cellulose (TMSC). TMSC was synthesized from microgranular cellulose by dissolving cellulose in lithium chloride in dimethylacetamide according to the procedure described in the literature.^{47,48,50} The clear solution was then heated to 80 °C followed by addition of hexamethyldisilazane (HMDS) in nitrogen atmosphere. In the reaction, HMDS substitutes the –OH groups on cellulose and forms TMSC that can easily be regenerated back to cellulose with HCl (Scheme 1). The solution was cooled, and TMSC

Scheme 1. Synthesis of TMSC from Cellulose Using HMDS and Regeneration Back to Cellulose with HCl



was crystallized. The TMSC was purified by dissolving in tetrahydrofuran and recrystallizing in methanol followed by filtration, washing several times with methanol, and drying in a desiccator. A degree of substitution (DS) of 2.5 was determined using liquid-state NMR (Bruker Avance III 500). All chemicals were purchased from Sigma-Aldrich, Germany.

Cellulose-Coated Si-Wafers (Si–CellOH). Hydrophobic cellulose and regenerated cellulose model surfaces for the captive bubble experiments were prepared according to a modified procedure previously described in the literature.⁵⁰ The model surfaces used in the captive bubble experiments were silicon wafers (Si-wafers, Okmetic, Espoo, Finland). The Si-wafers were first cleaned with a UV-ozone cleaner (Procleaner, BioForce Nanosciences, USA) for 10 min. Then, 3–4 drops of toluene was pipetted onto the wafer and spun for 30 s at 4000 rpm (WS-400BZ-6NPP/Lite, Laurell Technologies, USA). Hydrophobic cellulose surfaces were prepared by pipetting 3–4 drops of TMSC solution (10 g/L in toluene) onto the wafer and spinning for 1 min at 4000 rpm. The wafers were then dried in an oven at 60 °C for 10 min. The TMSC was regenerated back to cellulose by placing the TMSC-coated plates under HCl vapor in a desiccator for 7 min (Scheme 1). The HCl vapor was created by placing 200 mL of HCl (3.3 M) into the desiccator (size 200 DN) and sealing the lid. Partial regeneration of cellulose can be achieved by changing the regeneration time in HCl vapor.^{47–49} Cellulose-coated QCM-D SiO₂ crystals for the SDS adsorption experiments were prepared in a similar way to the Si-wafers.

Hydrophilic and Hydrophobic Modified Si-Wafers (Si–OH and Si–CH₃). Surface modification of the Si-wafers was performed according to a modified procedure previously described in the literature.⁵¹ First, the Si-wafers (10 × 10 mm) were cleaned with UV-light for 10 min. The Si-wafers were then hydrophilized by immersion in 2.5 M NaOH for 15 min. The NaOH treatment creates hydroxyl groups on the silica surface, making the surface highly hydrophilic (hydrophilic Si–OH). The slides were then rinsed thoroughly with water and dried with nitrogen gas. The wafers were kept in EtOH until use to avoid contamination.

Hydrophobization was conducted by treating the hydrophilized Si-wafers with a solution of 400 μL of CTMS in 10 mL of xylene overnight. CTMS treatment replaces the hydroxyl groups with dimethylsilyl groups on the silica surface, creating a hydrophobic surface (hydrophobic Si–CH₃). After the treatment, the slides were rinsed with xylene and dried with nitrogen gas.

Hydrophilic and Hydrophobic Modified QCM-D SiO₂ Crystals. These crystals for the SDS adsorption experiments were prepared in a similar way to the Si-wafers, with the difference that CTMS was drop casted onto the chip surface up to ca. seven drops and allowed to evaporate. The disposition process was repeated four times for the hydrophobic surfaces, and finally, the crystals were dried with nitrogen gas.

Methods. Determination of Contact Angle Using the Captive Bubble Method. Captive bubble measurements^{45,46} were carried out using an optical Theta tensiometer (Attension, Biolin Scientific,

Espoo, Finland). A model surface was first immersed (depth about 2 mm) horizontally in the liquid (see Figure 2a); then, a bubble

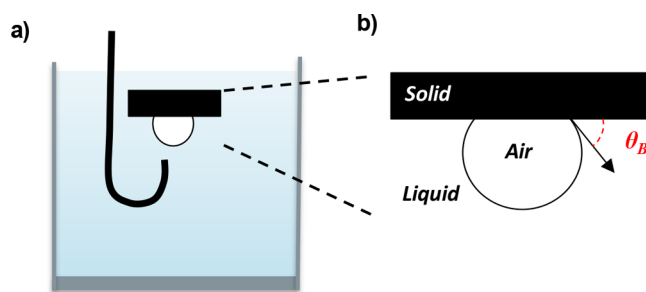


Figure 2. (a) Captive bubble method for determining the bubble contact angle (θ_B) against a solid surface: quartz cuvette with solution, hooked needle, model surface, and air bubble. (b) The contact angle is recorded from the outer edge of the bubble cross section.

(volume 4 μL) was created on the head of a hooked needle positioned beneath the surface. The bubble was allowed to stabilize for 600 s while the surface tension γ was recorded. After stabilization, the bubble was brought into contact with the model surface (10 mm/min), and if the bubble attached to the surface, the contact angle θ_B was recorded as the average over 60 s using images captured at a rate of 10 frames per second. The time scales of film rupture and bubble attachment shown later are rough estimates due to the limits of the used frame rate. The contact angle was recorded from both outer edges of the bubble (Figure 2b). Six replicates per test were conducted. The quartz cuvette and the hooked needle were carefully washed prior to and after every measurement using Deconex and EtOH and then rinsed with water. The experiments were carried out in a controlled atmosphere of 23 °C and 50% humidity.

Standard deviations (SD) of θ_B were approximately 6° with pure SDS and 10° with SDS and NaCl addition. The rather large SD is a reported drawback of the captive bubble method.^{52,53} Captive bubbles are sensitive to impurities and surface heterogeneity and roughness. Moreover, bubble asymmetry and variations in bubble size can alter the detected contact angle.⁵⁴ In addition, the measurement involves the use of a needle to attach the bubble on the surface, and wetting between the liquid and the needle can impact the results.^{52,55} In this study, the needle was retracted and detached from the bubble, which creates a pulling force and stretching of the bubble before detachment. In addition, the needle position in relation to the bubble during attachment contributes to the recorded values, and if the needle is off from the center line of the bubble the contact angles of different sides of the bubble will be different.⁵² These factors play a more important role when the surface tension is low. However, the relatively large SD did not hinder the interpretation of the results, as clear trends were observed.

Determination of Contact Angle and Surface Free Energy Using the Sessile Drop Method. An optical Theta tensiometer (Attension, Biolin Scientific, Espoo, Finland) and the sessile drop method were used to measure the contact angle and surface free energy of the modified surfaces. The unit includes a camera and lenses, a light source, and a sample stage. In the sessile drop measurement, a drop (4 μL) of liquid is placed onto a surface, and the shape of the liquid drop is recorded. The droplet contact angle (θ_D) is defined by the surface and the drop tangent. Under steady state, θ describes the surface wetting by the liquid according to Young's equation

$$\gamma_{SV} = \gamma_{SL} + \gamma_{LV} \cos \theta \quad (1)$$

where γ_{SV} is the surface free energy of the solid, γ_{SL} is the solid–liquid surface energy, γ_{LV} is the liquid surface tension, and θ is the measured contact angle of the drop. Surface free energy calculations of the model surfaces were carried out by measuring the contact angles with four different liquids: Milli-Q water, DIM, formamide, and ethylene glycol. Each contact angle value was the average of three measurements per surface. The experiments were carried out in a

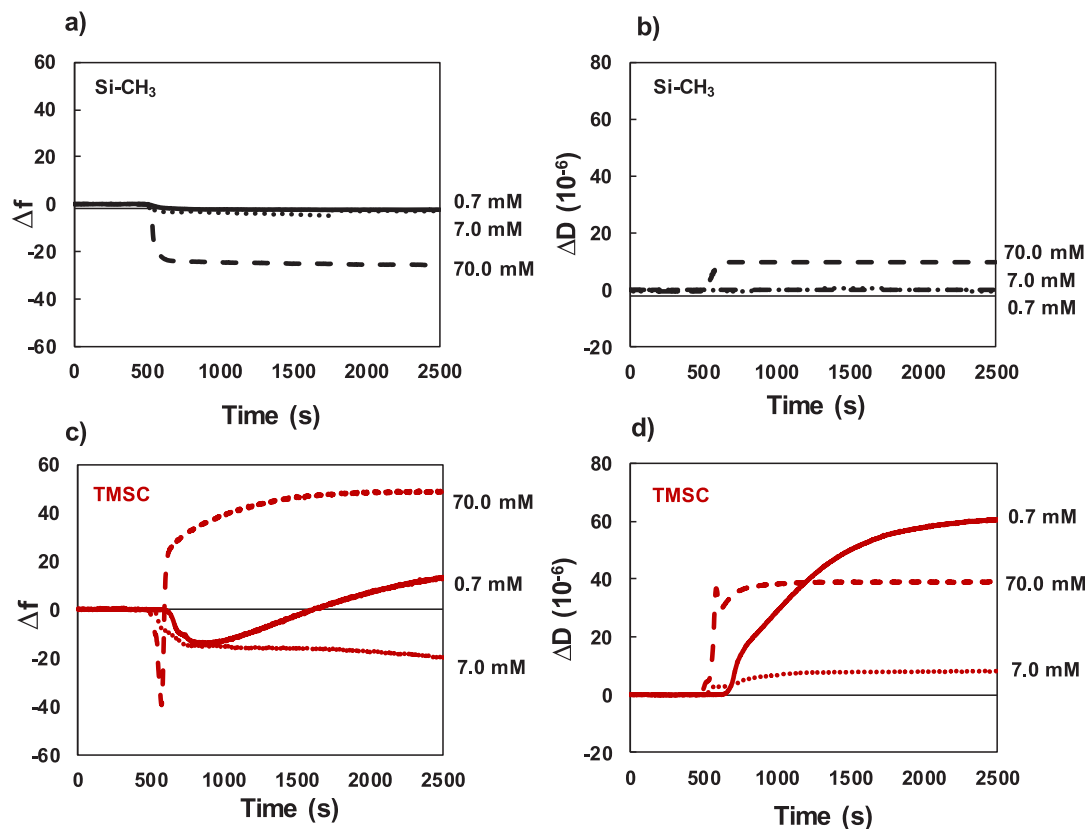


Figure 3. SDS adsorption isotherms for (a, b) hydrophobic silica (Si-CH₃) and (c, d) trimethylsilyl cellulose (TMSC) determined with QCM-D. SDS had concentrations of 0.7, 7.0, and 70.0 mM. Data illustrated as a third overtone number ($n = 3$), Δf is the change in the oscillation frequency in Hz, and ΔD is the dissipation. No rising step was included in the measurement.

controlled atmosphere of 23 °C and 50% humidity. Surface free energy was calculated using the OWRK/Fowkes method, which incorporates the contribution of polar γ_p and dispersive γ_d components in the total γ :

$$\gamma_{SL} = \gamma_{SV} + \gamma_{LV} - 2\sqrt{\gamma_{d,SV}\gamma_{d,LV}} - 2\sqrt{\gamma_{p,SV}\gamma_{p,LV}} \quad (2)$$

When combined with Young's equation (eq 1), eq 2 can be written as

$$\gamma_{LV}(1 + \cos \theta) = 2\sqrt{\gamma_{d,SV}\gamma_{d,LV}} + 2\sqrt{\gamma_{p,SV}\gamma_{p,LV}} \quad (3)$$

The components $\gamma_{d,SV}$ and $\gamma_{p,SV}$ are unknown. Thus, at least two liquids with polar and dispersive component need to be used for the calculations. A detailed description of the theory can be found elsewhere.⁵⁶

Surface Morphology and Roughness. An atomic force microscope (AFM, Analy instruments, afm+) was used to determine the morphology and roughness of the model surfaces. Silicon cantilevers (AppNano, ACTA-10, tip size <10 nm) were used in tapping mode for scanning with a resonance frequency of 200–400 kHz. Measurements were performed in air and at room temperature. Analysis studio software 3.11 was used to calculate surface roughness variation and root means square (RMS).

SDS Adsorption Isotherms. A quartz crystal microbalance with dissipation (QCM-D, Q-sense, Biolin Scientific, Espoo, Finland) was used to measure SDS adsorption on the modified QCM-D SiO₂ crystals, including hydrophobic and hydrophilic silica, TMSC, and cellulose. SDS concentrations of 0.7, 7.0, and 70.0 mM were tested. They correspond to values clearly below the critical micelle concentration (CMC) (ca. 8 mM, see Figure S1), close to CMC, and well above CMC. The crystals were first rinsed with water for 500 s as a baseline before injecting the SDS solution into the cell at a flow rate of 0.1 mL/min. The change in oscillation frequency (Δf) and dissipation (ΔD) caused by SDS adsorption was recorded for 30 min.

In the measurement, a reduction in frequency indicates adsorption, and increased dissipation relates to the structural changes of the adsorbed mass, such as the softening and thickening of adsorbed layers.

The Sauerbrey equation^{57,58} was used as an approximation to determine the apparent adsorbed mass (Δm) and apparent height (h) of the adsorbed layers according to eqs 4–5:

$$\Delta m = -C \frac{\Delta f}{n} \quad (4)$$

$$h = \frac{\Delta m}{\rho} \quad (5)$$

where C is a constant 17.7 ng/Hz·cm², Δf is the frequency change, n is the overtone of the oscillations, and ρ is the density of the substance. For SDS, a density value of 1.08 g/cm³ was used in the calculations.⁵⁹ We note that the Sauerbrey equation is more accurate for rigid thin films with low amounts of coordinated water in the structure and low viscoelasticity. Usually, if the dissipation is large compared to the frequency change, the film thickness needs to be determined by modeling; this was not conducted within this study, and the data thus need to be compared on a relative basis.

RESULTS AND DISCUSSION

Model Surface Characteristics and SDS Adsorption Isotherms. The surface hydrophobicity, surface free energies, and roughness of the surfaces are listed in Table 1, and AFM images are shown in Figure S3. This includes similar energy values for both hydrophobic surfaces (silica and TMSC) and also for both hydrophilic surfaces (silica and cellulose). Cellulose had a higher dispersive component than hydrophilic silica due to the amphiphilic nature of the cellulose

molecule.^{60,61} In agreement with earlier measurements,^{35,51} we found a similar difference between dispersive components of hydrophilic and hydrophobic silica. The roughness variation of the surfaces was small, and all other surfaces except the partially desilylated TMSC surface can be considered to be smooth. The RMS roughness was 18.4 nm for the TMSC surface with $\theta_D \sim 75^\circ$, and the formation of spherical aggregates of ~ 200 nm diameter was observed. The effect of roughness is discussed more closely in the section “Pinning of the Three-Phase Contact Line during Bubble Attachment to TMSC”.

SDS adsorption on the model surfaces was studied to understand its possible contribution to the bubble–surface interaction. The SDS isotherms for adsorption on the hydrophobic model surfaces (Si–CH₃ and TMSC) are shown in Figure 3, and the calculated changes in mass and height (eqs 4 and 5) of the adsorbed layers are presented in Table S1. With Si–CH₃ at a concentration below the CMC, the changes in frequency and dissipation (Figure 3a, b) were small but detectable. Close to the CMC, the larger SDS adsorption affected both frequency and dissipation, even though the above frequency change was rather small ($\Delta f \approx -4$ Hz) when compared to the effect of larger molecules. Above the CMC, the bound water in absorbing SDS micelles caused a high final dissipation. The stabilization of SDS adsorption was reached within 5 min.

SDS adsorption on the hydrophobic silica surface can be explained by the hydrophobic interaction between the surface and hydrophobic tail of SDS.^{62–64} Figures 3a and 3b agree with previous SDS adsorption studies on other hydrophobic surfaces,^{63,65–67} where SDS adsorbs as single monomers below 2 mM concentration and as hemimicelles at higher concentration until the surface is saturated at 7 mM. Thus, the high dissipation measured at 70 mM of SDS indicates that there is micelle formation on the surface but also water coordination on the adsorbed layer.

SDS adsorption on TMSC (Figure 3c, d) differed greatly from the adsorption on hydrophobic silica. At a concentration below the CMC, the SDS adsorption was first seen as a clear decrease in frequency and as an increase in dissipation as expected. However, the subsequent transients could result from slowly diffusing and organizing SDS molecules within the chemically heterogeneous TMSC surface.⁶⁸ The mass loss after 800–900 s (Δf increased) suggests that SDS replaced bound water at the surface, where dissipation ΔD was still increasing. In other words, a low amount of SDS monomers in the solution seems to cause competitive adsorption of SDS and water molecules on the surface, seen as a simultaneous increase in both frequency and dissipation. Steady state was not reached within the measurement time, which could require several days in this kind of unstable system.

Close to the CMC, SDS adsorption on TMSC was much more stable, suggesting a fairly uniform adsorbed layer, likely comprised of SDS monomers. However, above the CMC, a rapid transient drop in frequency was followed by an increase during the remaining monitoring time. At the same time, the dissipation ΔD approached a steady value. This suggests that the SDS micelles released or replaced bound water after adsorption similarly to the earlier case of low SDS concentration. TMSC is a chemically heterogeneous surface with a measured high DS value of 2.5. Thus, even though the surface is mainly hydrophobic ($\theta_D = 93^\circ$), there are still free hydroxyl groups that can bind water. This feature is related to

the long time (24 h) required for stabilization of the frequency baseline before QCM-D data acquisition.

The SDS isotherms for adsorption on the hydrophilic model surfaces (Si–OH and cellulose) are shown in Figure S4, and the calculated changes in mass and height (eqs 4 and 5) of the adsorbed layers are presented in Table S1. At a concentration below the CMC, the changes in frequency and dissipation were slightly lower than with hydrophobic silica but still detectable. Close to the CMC, SDS adsorption on cellulose was similar to that on hydrophobic silica. In contrast, the adsorption on hydrophilic silica was minor at equal SDS concentrations. Above the CMC, SDS adsorbed on both hydrophilic surfaces with a large increase in dissipation. Steady state was reached within 5 min for cellulose, whereas for hydrophilic silica it was reached after 30 min.

Electrostatic repulsion explains the negligible adsorption of negatively charged SDS on hydrophilic silica below the CMC (Figure S4).⁶⁹ Increased SDS adsorption with an increase in SDS concentration on a hydrophilic surface could be caused by electrostatic screening of the charges in the presence of counterions (Na⁺) in solution.^{64,70,71} However, most of the mass gains are explained by the hydration water,⁵⁹ which correlated with the observed high dissipation.

Electrostatic Bubble Repulsion for Smooth Hydrophilic Surfaces. Bubble interaction with smooth hydrophilic surfaces was investigated using the captive bubble method. The bubbles did not attach to hydrophilic silica or cellulose immersed in water or in SDS solution; i.e., the wetting film between the bubble and hydrophilic surface remained stable (Figure 4). Moreover, the cellulose surfaces were measured both after 10 min and overnight immersion in water. We note that the prolonged immersion did not influence the observed behavior.

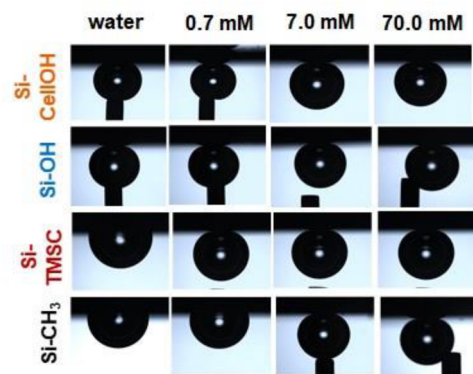


Figure 4. Bubbles captive on cellulose (Si–CelloH and Si–TMSC) and modified silica (Si–OH and Si–CH₃) surfaces at SDS concentrations of 0, 0.7, 7.0, and 70.0 mM. No bubble attachment was observed on hydrophilic Si–OH or Si–CelloH surfaces. In contrast, the bubble attached to hydrophobic Si–TMSC and Si–CH₃ surfaces by rupturing the wetting film at the lowest SDS concentration used. However, the wetting film became stable at higher SDS concentrations.

Bubble surfaces are negatively charged in water^{21,72} and in SDS solution,¹⁷ and therefore the bubbles strongly repel the fully wetted hydrophilic surface. Despite the amphiphilicity of cellulose, the hydrophilic character dominated the bubble–surface interaction. The presence of hydrophobic domains was indicated by the QCM-D measurements (Figure S4c,d)

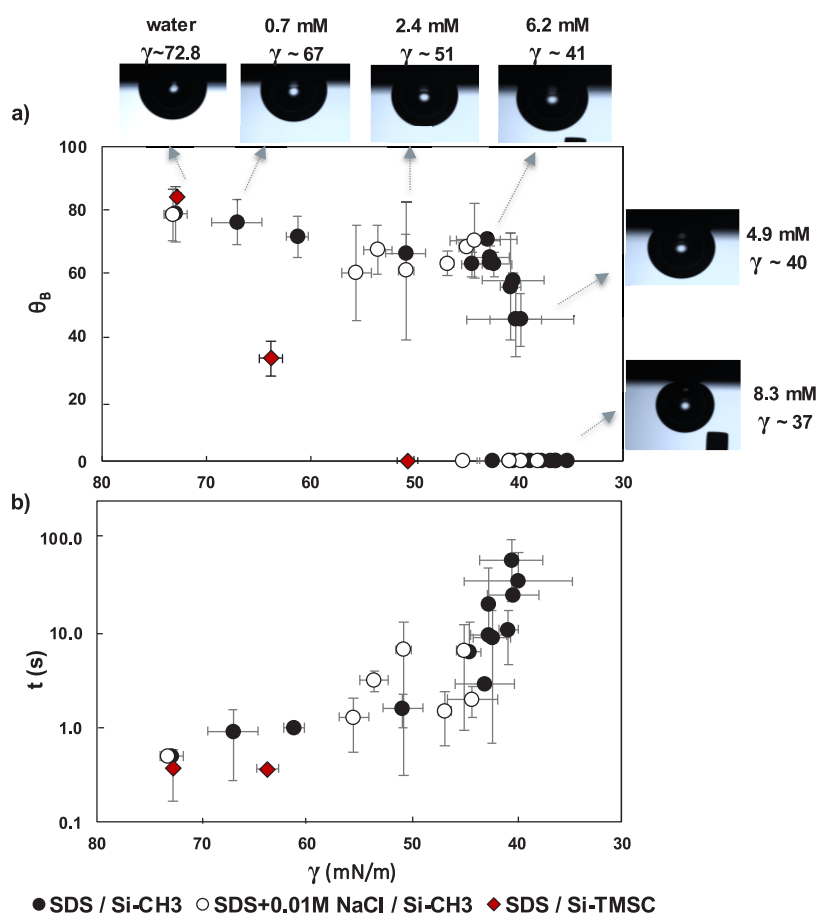


Figure 5. (a) Surface contact angle θ_B (°) measured with the captive bubble method as a function of surface tension γ . (b) Average time (seconds) of bubble attachment on Si-TMSC (red diamond) and Si-CH₃ (●) surfaces as a function of surface tension γ in pure SDS solution. Si-CH₃ surfaces were also measured in SDS solution with 0.01 M NaCl addition (○). The situation with no attachment on Si-CH₃ is indicated as $\theta_B = 0^\circ$. Error bars indicate the standard deviation.

showing SDS adsorption on the regenerated cellulose near the CMC. SDS penetrates into the cellulose film and turns it even more hydrophilic as the hydrophobic domains are filled with SDS.⁷³

Critical Surface Tension for Bubble Attachment on Smooth Hydrophobic Surfaces. The wetting film stability and bubble attachment time on smooth hydrophobic silica and TMSC were studied more closely using the captive bubble method (Figures 4 and 5). The aim of these experiments was to determine the critical surface tension for wetting transition by changing the SDS concentration. The effect of the electrolyte was also determined for hydrophobic silica. The addition of 0.01 M NaCl was chosen as it is known to have a moderate effect on surface tension when added with SDS (Figure S1).⁷⁴ This detectable but not too strong effect enables the production of a controlled surface tension isotherm.⁶³ Theoretical models were used to compare and explain the observed results. We first discuss the results for hydrophobic silica and then for TMSC surfaces, pointing out the mechanisms that explain the observed behaviors.

Bubble Interaction with Hydrophobic Silica, Si-CH₃. Figure 5 summarizes the changes in bubble contact angle θ_B and attachment time as a function of surface tension. The addition of SDS decreased both γ and θ_B , while the bubble attachment time increased. Possible scenarios for SDS adsorption on the hydrophobic surface and at the air-liquid

interface affecting bubble-surface interaction are presented in Figure 6. At a SDS concentration of 3.5 mM, bubble

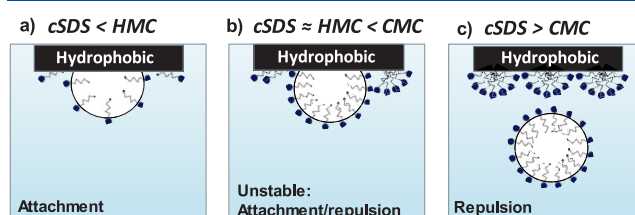


Figure 6. Possible scenarios for SDS adsorption on a hydrophobic surface and at the air-liquid interface along with its effect on bubble-surface interaction. HMC stands for the critical hemimicelle concentration (2 mM for SDS).^{63,66} CMC is the critical micelle concentration (8.2 mM for SDS).

attachment probability decreased significantly. At this concentration, the air-water interface is almost fully covered with SDS (Figure S2), and hemimicelles form on the Si-CH₃ surface (see Figure 6b). No bubble attachment occurred beyond 6.9 mM. This level is roughly the same as the threshold for micelle formation in the solution (see Figure 6c).^{63,66} The critical surface tension value of $\gamma = 37$ mN/m is not directly explained by the equilibrium spreading coefficient derived from eq 1⁴² but also requires consideration of the friction of the moving contact line, as explained in the next section.

The presence of NaCl (0.01 M) slightly increased the bubble attachment time but did not have a significant effect on θ_B when compared to a pure SDS solution of similar surface tension. The bubbles no longer attached to the surface when the surface tension was about 40 mN/m. However, the SDS concentration was only 2.8 mM at this point. Both surface tension and CMC decreased with added NaCl (Figure S1) due to the electrostatic screening of negative charges by the positive counterions (Na^+). Essentially, more SDS molecules were able to pack at the air–water interfaces.⁷⁴

Theoretical Considerations on Wetting Transition on Si–CH₃. Here we estimate the energy changes of the immersed hydrophobic silica surface at different surfactant concentrations and compare these to the measured surface free energy of 22.0 mN/m (solid–vapor surface energy, γ_{SV}) (Table 1). During bubble attachment a new solid–vapor interface is formed, and therefore, the bubble contact angle θ_B effectively corresponds to the *receding* contact angle of a drop on the chemically homogeneous surface. A force balance along the solid homogeneous surface leads in this dynamic case to the following equation:⁷⁵

$$2\gamma_{SV} = \gamma_{SL} + \gamma_{LV}\cos(\theta_B) \quad (6)$$

where γ_{SV} is the surface free energy of the solid, γ_{SL} is the solid–liquid surface energy, γ_{LV} is the liquid surface tension, and θ_B is the measured contact angle of the bubble. The average frictional tension of the moving three-phase contact line during attachment leads to an extra γ_{SV} factor on the left-hand side of the equation (compare with eq 1). The somewhat phenomenological eq 6 has earlier been used to explain, surprisingly well, the contact angle hysteresis,⁷⁵ where nonequilibrium phenomena, like friction, play an important role. In particular, the precursor film near a moving three-phase contact does not seem to alter the above average friction, although this term neglects all nanoscale features of the problem. We apply a similar approach to an attached bubble, omitting finer details arising from a possible thin liquid film between the bubble and the solid surface.⁴³

Using the measured values of surface free energy, surface tension, and θ_B , eq 6 provide us with an estimate of the effective value of γ_{SL} . The effective γ_{SL} of the immersed surface in water is 29.7 mN/m. Figure 7 shows how γ_{SL} approaches the

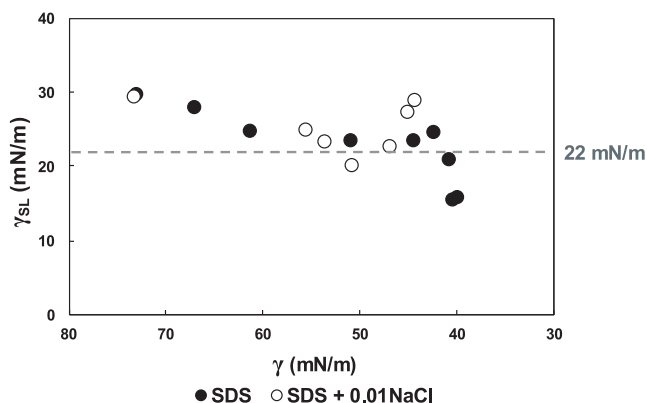


Figure 7. Solid–liquid surface energy (γ_{SL}) of the immersed Si–CH₃ surface as a function of surface tension (γ) estimated based on eq 6. γ_{SL} approaches the measured surface free energy (γ_{SV}) of 22.0 mN/m (dashed line) near the transition for both pure SDS solution (filled dots) and the solution with added NaCl (open dots).

surface free energy of 22.0 mN/m near the wetting transition for the pure SDS solution. With added NaCl, there is more scatter in the data near the transition, but the overall trend is similar. The critical value of the surface tension $\gamma \approx 40$ mN/m suggests that the value of the bubble contact angle θ_B (solved from eq 6) is $\arccos(22/40)$ radians, i.e., 57° , at the first-order transition. This estimate agrees well with the result of the captive bubble measurement (Figure 5).

Changes in interfacial and surface energies caused by the bubble attachment and its effect on the total interface energy of the system (E_{tot}) can be considered using eq 6 together with simple bubble geometry (see the Supporting Information). The calculated (free) bubble interface energy in water was relatively high, ca. 900 nJ. The total interface energy of the system (E_{tot}) is reduced when the bubble attaches to the surface.⁷⁶ In water, the energy reduction was 208 nJ (Figure S7), and the addition of SDS decreased this value. A steep decrease in ΔE_{tot} occurred after an SDS concentration of 3.5 mM ($\gamma = 45$ mN/m), which is the concentration where the air–water interface is almost fully covered with SDS, and bubble behavior shifts from clear attachment to more scattered. After ΔE_{tot} of 45 nJ at $\gamma = 40$ mN/m (close to the CMC of SDS), bubble attachment no longer occurred, and the system reached its energy minimum. No electrostatic forces were considered in these calculations.

Bubble Interaction with Hydrophobic TMSC. The bubble interaction with the hydrophobic TMSC surface in water was similar to that with hydrophobic silica (Figure 5). Using eq 1 and the estimates $\theta_B = 96.8^\circ$ and $\gamma_{SV} = 21.38$ mN/m for the pure TMSC surface,⁴⁹ we obtain the estimate of $\gamma_{SL} = 30$ mN/m for the solid–liquid surface energy in water. Taking into account the friction of the moving three-phase contact line, these numbers together with eq 6 lead to a predicted $\theta_B \approx 80^\circ$ for an attaching bubble in pure water. For the TMSC surface, the measured contact angle 85° was thus not only close to the predicted value but also very near the measured angle, 79° , for the hydrophobic silica. This is explained by the similar hydrophobicity and dispersive and polar components of TMSC and hydrophobic silica surfaces (see Table 1).

However, contrary to measurements for hydrophobic silica, the addition of SDS had a significant effect on the bubble behavior for TMSC already at very low concentration (Figure 5). At a SDS concentration of 1.0 mM ($\gamma = 64 \pm 2$ mN/m), θ_B was already rather low, $33 \pm 6^\circ$ (compare with 72° for hydrophobic silica at equal concentration). Due to this low value, it was difficult to clearly observe the rupture of the wetting film. With increased SDS concentration, 2.4 mM, the wetting film remained stable, with no signs of bubble attachment. The critical value of the surface tension was in the range of 50–60 mN/m for the pure SDS solution. This critical value was considerably higher for the TMSC surface than for hydrophobic silica.

A different response to changes in SDS concentration was expected due to the more complex SDS absorption (Figure 3). The above large decay in θ_B with added SDS and the much higher critical surface tension for amphiphilic TMSC can be explained by a larger frictional tension of the moving contact line on the TMSC surface. The higher frictional tension balances the larger surface tension in an equation similar to eq 6. A more detailed quantitative analysis of this issue is presented in the next section.

Critical Hydrophobicity of Cellulose for Bubble Attachment. Critical hydrophobicity of cellulose surfaces

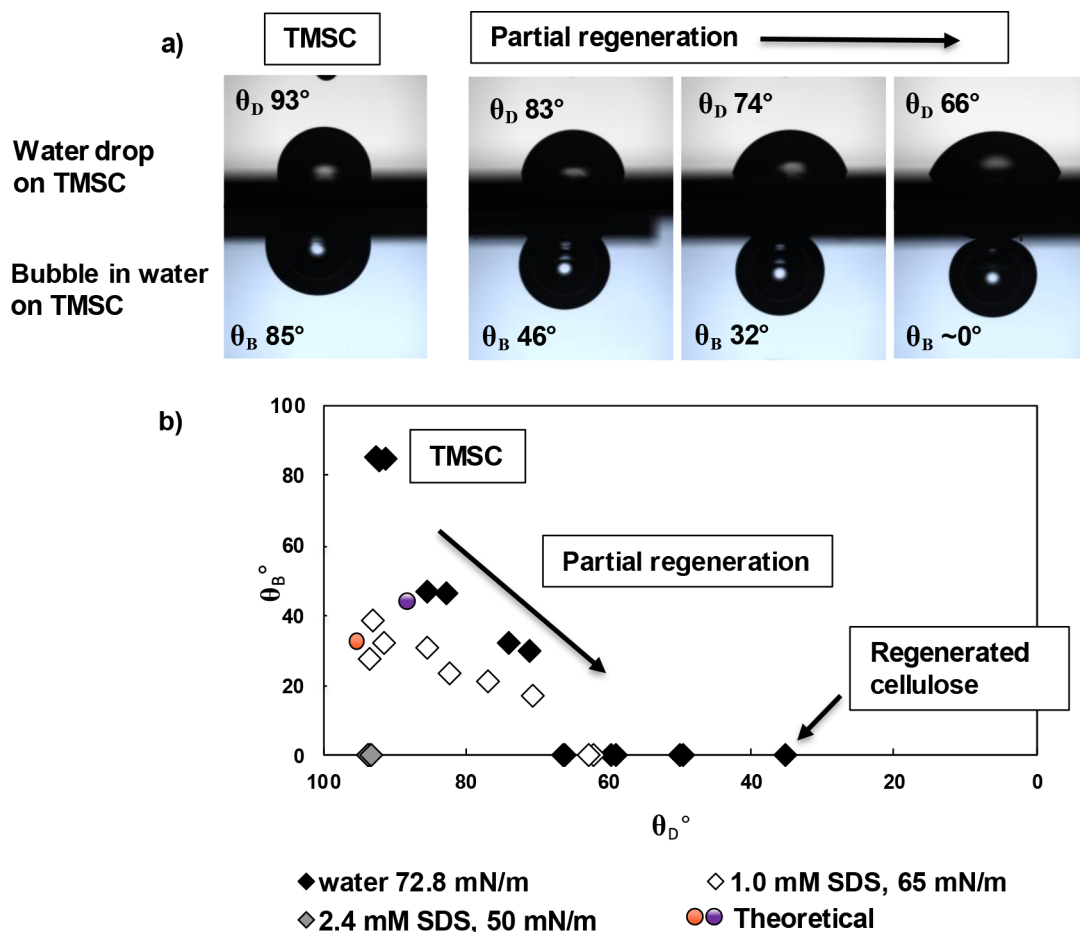


Figure 8. (a) Sessile drop (θ_D) and captive bubble (θ_B) contact angles of pure Si–TMSC and partial regenerated TMSC surfaces with decreasing contact angles described from left to right as the regeneration proceeds. When θ_D was around 65° the bubbles no longer attached to the surface. (b) Effect of partial regeneration of TMSC on θ_D and θ_B measured with water (black diamond), 1.0 mM of SDS (white diamond), and 2.4 mM of SDS (gray diamond). Cases with no bubble attachment are indicated as $\theta_B = 0^\circ$. Orange (SDS) and violet (water) dots show the theoretical predictions of the effects of slight surface regeneration or small SDS addition on the θ_B change due to pinning of the three-phase contact line.

for bubble attachment was determined experimentally using partially regenerated TMSC surfaces⁴⁹ with θ_D of ca. 85° , 75° , 65° , 60° , 50° , and 35° . These values should be compared with θ_D of 93° for the pure TMSC surface. Fully regenerated cellulose (all methylsilyl groups desilylated to $-\text{OH}$ groups) had θ_D of 35° . Surface contact angles in water and in SDS solution (1.0 mM) were also measured with the captive bubble (θ_B). The results in Figure 8 show a rather large difference between θ_B and θ_D for partially regenerated TMSC surfaces. The 8° difference for pure TMSC in water increased to almost 40° for regenerated TMSC when θ_D was in the range of 70 – 85° . The presence of SDS (1.0 mM) increased the difference between θ_B and θ_D , up to 50 – 60° for both partially regenerated and also pure TMSC surfaces. The differences between θ_B and θ_D can be explained by a contact angle hysteresis^{45,53} for a chemically heterogeneous surface with pinning sites for the three-phase contact line (see the section **Pinning of the Three-Phase Contact Line during Bubble Attachment to TMSC**). Bubbles did not attach to the surface when θ_D was 60 – 65° or below. However, even in this region, bubbles elongated during the retraction, indicating some adhesion to the surface. Further discussion on this phenomenon is presented in the **Supporting Information** (Figure S5). In this study, only fully attached bubbles were considered in the theoretical calculations.

Pinning of the Three-Phase Contact Line during Bubble Attachment to TMSC. Gradual regeneration of the TMSC surface creates an increasing number of cellulose $-\text{OH}$ groups, which are a source of chemical heterogeneity of the surface.^{49,53} In other words, partial regeneration creates a hydrophobic (1) surface with hydrophilic (2) microscopic domains, as depicted in Figure 9. Earlier Lattice Boltzmann simulations⁷⁷ have shown a pinning of the three-phase contact line on such hydrophobic–hydrophilic boundaries. The pinning affects the frictional tension during the initial dewetting of the solid surface required for the bubble attachment. In analogy to eq 6, the threshold to overcome the pinning tension for heterogeneous surfaces can be described by the equation

$$\gamma_{SV,1} + \gamma_{SV,2} = \gamma_{SL,1} + \gamma_{LV} \cos \theta_r \quad (7)$$

where $\gamma_{SV,i}$ is the surface free energy of the solid of type i , $\gamma_{SL,i}$ is the respective solid–liquid surface energy, γ_{LV} is the liquid surface tension, and θ_r corresponds to the receding contact angle (i.e., θ_B) determined by the surface energies on both sides of the pinning site (see Figure 9). We assume in eq 7 that the main friction $\gamma_{SV,2}$ of the moving contact line comes from hydrophilic microscopic domains of type 2 on the otherwise hydrophobic surface (1).

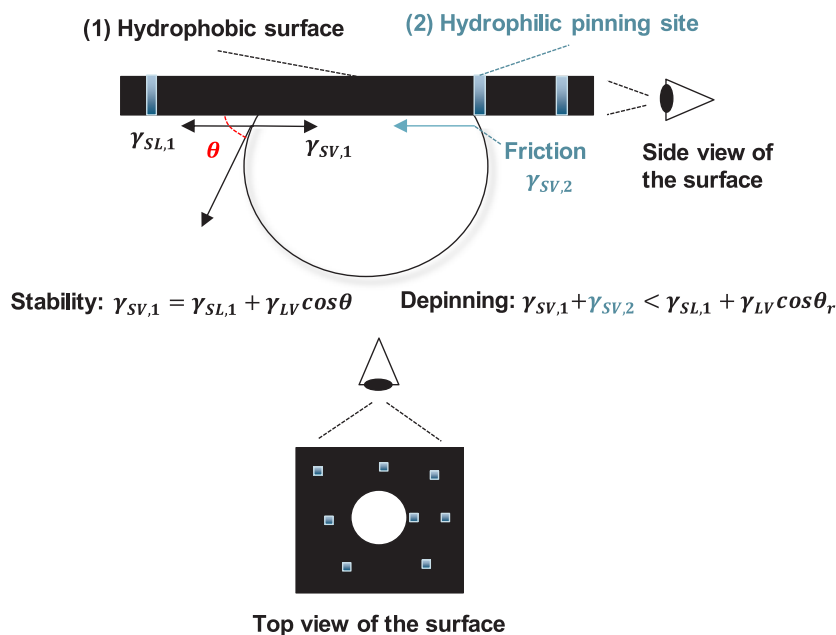


Figure 9. Pinning of the three-phase contact line on a hydrophobic (1) surface with hydrophilic (2) microscopic domains. Depinning requires that the tensions coming from surface and interface energies overcome the friction $\gamma_{SV,2}$, which is the surface free energy of the hydrophilic domain. $\gamma_{SL,1}$ is the solid–liquid surface energy of surface (1), γ_{LV} is the liquid surface tension, and θ_r corresponds to the receding contact angle (i.e., θ_B).

Equation 7 was used for the theoretical prediction of the effect of partial regeneration and SDS concentration on the θ_B of TMSC surfaces. As explained earlier, eq 6 predicted $\theta_B \approx 80^\circ$ for the homogeneous hydrophobic TMSC surface in water. This should be compared with the value of $\theta_B \approx 45^\circ$ obtained from eq 7 for a heterogeneous, partly regenerated surface comprised of estimates of $\gamma_{SV,1} = 21.38$ mN/m, $\gamma_{SL,1} = 30$ mN/m for TMSC and $\gamma_{SV,2} = 60$ mN/m for cellulose. The prediction thus shows a rapid drop in bubble contact angle ($\theta_B \approx 80^\circ \rightarrow 45^\circ$) when moving from a hydrophobic TMSC surface to a slightly regenerated one (Figure 8). This kind of drop was observed experimentally, from $\theta_B \approx 85^\circ$ to $\theta_B \approx 47^\circ$ for a surface regenerated over a short time (2–3 min). Interestingly, the close agreement between the theoretical prediction and our experiment was obtained without the inclusion of a differential Cassie factor^{75,78} in eq 7. The reason could be the pointwise nature of the hydrophilic domains on an otherwise hydrophobic surface so that their total area remains low even when they cover the surface densely.

Equation 7 could also be used to describe the high sensitivity of the bubble contact angle on liquid surface tension. At a SDS concentration of 1.0 mM, eq 7 gives the theoretical value of $\theta_B \approx 36^\circ$ for the hydrophobic TMSC surface using the measured value $\gamma = 64 \pm 2$ mN/m for the liquid surface tension and estimating other surface energies as done earlier. This theoretical prediction compares well with the experimental value of $33 \pm 6^\circ$ for θ_B (Figure 8). Moreover, we used the same surface energy $\gamma_{SV,2} = 60$ mN/m in eq 7 to estimate θ_B as earlier in the case of hydrophilic pinning domains caused by regeneration. This suggests that the efficient adsorption of SDS on the hydrophobic TMSC surface (see Figure 3) creates similar hydrophilic pinning sites as the partial regeneration of this surface.

Plotting the effective $\gamma_{SL,1}$ solved from eq 7 for the partially regenerated TMSC surfaces shows (Figure 10) that this energy meets the surface free energy of the fully hydrophobized TMSC surface slightly before the actual wetting transition at

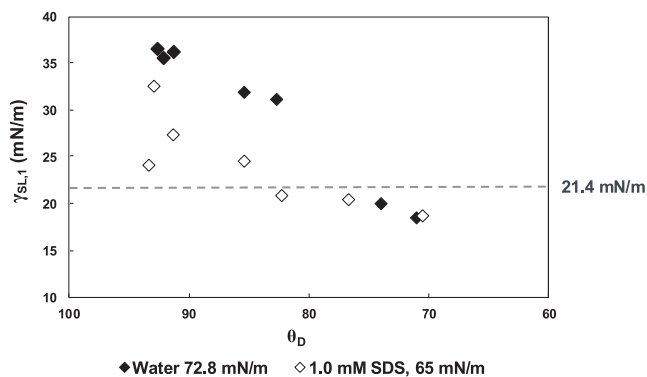


Figure 10. Solid–liquid surface energy $\gamma_{SL,1}$ of the partial regenerated TMSC surfaces measured with water (black diamond) and 1.0 mM of SDS (white diamond) for different levels of hydrophobicity as described by the contact angle θ_D ($^\circ$) of a sessile drop. The estimate of $\gamma_{SL,1}$ obtained from eq 7 is near the surface free energy $\gamma_{SV,1} = 21.38$ mN/m of the fully hydrophobic TMSC surface in the vicinity of the critical hydrophobicity.

$\theta_D = 65^\circ$. This discrepancy could be caused by the fact that Figure 10 neglects the effect of small surface roughness. A RMS roughness of 18.4 nm was found by AFM imaging for the partially regenerated TMSC surface at $\theta_D = 75^\circ$ (Figure S3) due to formation of spherical aggregates (average diameter ca. 200 nm). The observed value of θ_B is thus slightly smaller than the corresponding intrinsic contact angle. Using Wenzel's formula $\cos(\theta_r) = \cos(\theta_B)/r$ to correct this in eq 7 leads to higher estimates of the effective $\gamma_{SL,1}$. The roughness factor r obtained from the measured AFM profile (Figure S3) is rather small, on average 1.002 with a maximal local value of 1.02. Having intersection with the surface free energy 21.4 mN/m at 65° would require a larger value of 1.07 in Wenzel's formula. Thus, roughness alone is not sufficient to explain why the effective $\gamma_{SL,1}$ crosses over 21.4 mN/m at a larger θ_D angle. A further reason for the discrepancy could be that eq 7 neglects

the nanoscale wetting film under a bubble,⁴³ covering partly the pinning sites and thus diminishing their effect.

CONCLUSIONS

Bubble attachment on regenerated cellulose and modified silica surfaces of different degrees of hydrophobicity was studied to reveal the key mechanisms involved in complex bubble–fiber interactions. Generally, bubbles immersed in water were subjected to repulsive interactions with hydrophilic silica and cellulose surfaces but were attractive with hydrophobic surfaces. The presence of SDS turned the attractive interaction between hydrophobic silica and a bubble into repulsion when the surface tension was around 40 mN/m, and the attachment tendency showed significant scatter near the transition. Moreover, the critical SDS concentration was affected by the electrolyte concentration. Due to efficient SDS adsorption on hydrophobic TMSC, the critical surface tension was higher at 50–60 mN/m. On the other hand, the transition for bubble attachment in water, at a critical drop contact angle of 65°, was determined by changing the surface energy of TMSC by partial regeneration.

The role of various interaction components was analyzed theoretically in terms of calculated surface and interface energies. This required not only considering the energy balance at the steady state but also that of the dynamics, which includes the moving three-phase contact line of an attaching bubble. Therefore, it was necessary to add frictional tension to the Young's equation describing the dynamic case. The frictional term differed for chemically homogeneous and heterogeneous surfaces due to pinning of the contact line in the latter. When separating the two cases, we were able to predict the observed dramatic drop in bubble contact angle caused by either regeneration of the TMSC surface or the addition of SDS. In contrast to previous literature, this prediction did not require explicit consideration of electrostatic forces.

Based on the results presented here, smooth cellulose surfaces are not expected to attract air bubbles in wet fiber foams. The surface needs to have a rather high hydrophobic content until a clear attractive interaction occurs, and the presence of surfactants and electrolytes can weaken the interaction considerably. In applications such as textile fabric manufacture,⁷⁹ with both natural and man-made fibers, the foam-formed structure is expected to be sensitive not only to the type of fibers used but also to the type and concentration of surfactant. The pinning of bubbles to fibers contributes, among other things, to the coarsening of wet fiber foams and thus to their drainage properties.⁷ SDS was shown to adsorb on both hydrophilic and hydrophobic cellulose, which can also affect the dry material properties.⁸⁰ The roles of nanobubbles and surface roughness on bubble–fiber interaction remain open questions. Accordingly, the connection between wet foam and dry fiber network properties needs to be investigated. The present findings can be applied to a better understanding of the forming processes with smooth fibers, opening ways to produce new foam-formed fiber materials.^{2,3}

ASSOCIATED CONTENT

Supporting Information

The Supporting Information is available free of charge at <https://pubs.acs.org/doi/10.1021/acs.langmuir.0c00682>.

Surface tension isotherms of SDS; calculated SDS adsorption at the air–water interface; model surface characteristics; SDS isotherms for adsorption on the model surfaces; bubble adhesion on partially regenerated cellulose; calculated changes in interface and surface energies due to an attaching bubble for varied surface tension (PDF)

AUTHOR INFORMATION

Corresponding Author

Jukka A. Ketoja – VTT Technical Research Centre of Finland Ltd., FI-02150 Espoo, Finland; orcid.org/0000-0002-8260-4267; Email: jukka.ketoja@vtt.fi

Authors

Annika E. Ketola – VTT Technical Research Centre of Finland Ltd., FI-02150 Espoo, Finland

Wenchao Xiang – Department of Bioproducts and Biosystems, School of Chemical Engineering, Aalto University, FI-00076 Espoo, Finland; orcid.org/0000-0003-4281-3109

Tuomo Hjelt – VTT Technical Research Centre of Finland Ltd., FI-02150 Espoo, Finland

Heikki Pajari – VTT Technical Research Centre of Finland Ltd., FI-02150 Espoo, Finland

Tekla Tammelin – VTT Technical Research Centre of Finland Ltd., FI-02150 Espoo, Finland; orcid.org/0000-0002-3248-1801

Orlando J. Rojas – Department of Bioproducts and Biosystems, School of Chemical Engineering, Aalto University, FI-00076 Espoo, Finland; Departments of Chemical & Biological Engineering, Chemistry, and Wood Science, The University of British Columbia, Vancouver, British Columbia V6T 1Z3, Canada; orcid.org/0000-0003-4036-4020

Complete contact information is available at: <https://pubs.acs.org/10.1021/acs.langmuir.0c00682>

Notes

The authors declare no competing financial interest.

ACKNOWLEDGMENTS

This work was supported by the Academy of Finland (Grant Nos. 296846 and 296851, Project “Surface interactions and rheology of aqueous cellulose-based foams”). We are also grateful for the support of the FinnCERES Materials Bioeconomy Ecosystem. W.X. and O.J.R. acknowledge the European Research Council (ERC) under the European Union's Horizon 2020 research and innovation program (ERC Advanced Grant Agreement No. 788489, “BioElCell”). The authors thank Vuokko Liukkonen for her kind help and assistance with the Theta instrument, Katja Pettersson for AFM imaging of the model surfaces, and Katri Kontturi for guidance and support with the QCM-D measurements.

REFERENCES

- (1) Radvan, B.; Gatward, A. P. J. The Formation of Wet-Laid Webs by a Foaming Process. *Tappi* **1972**, *55* (5), 748–751.
- (2) Lehmonen, J.; Rantanen, T.; Kinnunen-Raudaskoski, K. Upscaling of Foam Forming Technology for Pilot Scale. *Tappi J.* **2019**, *18* (8), 461–474.
- (3) Kiiskinen, H.; Salminen, K.; Lappalainen, T.; Asikainen, J.; Keränen, J.; Hellén, E. Progress in Foam Forming Technology. *Tappi J.* **2019**, *18* (8), 499–510.

- (4) Jahangiri, P.; Madani, A.; Korehei, R.; Zeinoddini, S. S.; Martinez, D. M.; Olson, J. A.; Sharma, Y.; Phillion, A. On Filtration and Heat Insulation Properties of Foam Formed Cellulose Based Materials. *Nord. Pulp Pap. Res. J.* **2014**, *29* (4), 584–591.
- (5) Madani, A.; Zeinoddini, S.; Varahmi, S.; Turnbull, H.; Phillion, A. B.; Olson, J. A.; Martinez, D. M. Ultra-Lightweight Paper Foams: Processing and Properties. *Cellulose* **2014**, *21* (3), 2023–2031.
- (6) Härkäsalmi, T.; Lehmonen, J.; Itälä, J.; Peralta, C.; Siljander, S.; Ketoja, J. A. Design-Driven Integrated Development of Technical and Perceptual Qualities in Foam-Formed Cellulose Fibre Materials. *Cellulose* **2017**, *24* (11), 5053–5068.
- (7) Whyte, D.; Haffner, B.; Tanaka, A.; Hjelt, T.; Hutzler, S. Interactions of Fibres with Simple Arrangements of Soap Films. *Colloids Surf., A* **2017**, *534*, 112–119.
- (8) Xiang, W.; Preisig, N.; Laine, C.; Hjelt, T.; Tardy, B. L.; Stubenrauch, C.; Rojas, O. J. Surface Activity and Foaming Capacity of Aggregates Formed between an Anionic Surfactant and Non-Cellulosics Leached from Wood Fibers. *Biomacromolecules* **2019**, *20* (July), 2286–2294.
- (9) Al-Qararah, A. M.; Hjelt, T.; Koponen, A.; Harlin, A.; Ketoja, J. A. Response of Wet Foam to Fibre Mixing. *Colloids Surf., A* **2015**, *467*, 97–106.
- (10) Al-Qararah, A. M.; Hjelt, T.; Koponen, A.; Harlin, A.; Ketoja, J. A. Bubble Size and Air Content of Wet Fibre Foams in Axial Mixing with Macro-Instabilities. *Colloids Surf., A* **2013**, *436*, 1130–1139.
- (11) Järvinen, M.; Pihko, R.; Ketoja, J. A. Density Development in Foam Forming: Wet Pressing Dynamics. *Nord. Pulp Pap. Res. J.* **2018**, *33* (2), 226–236.
- (12) Paunonen, S.; Timofeev, O.; Torvinen, K.; Turpeinen, T.; Ketoja, J. A. Improving Compression Recovery of Foam-Formed Fiber Materials. *BioResources* **2018**, *13* (2), 4058–4074.
- (13) Burke, S. R.; Möbius, M. E.; Hjelt, T.; Hutzler, S. Properties of Lightweight Fibrous Structures Made by a Novel Foam Forming Technique. *Cellulose* **2019**, *26* (4), 2529–2539.
- (14) Al-Qararah, A. M.; Ekman, A.; Hjelt, T.; Kiiskinen, H.; Timonen, J.; Ketoja, J. A. Porous Structure of Fibre Networks Formed by a Foaming Process: A Comparative Study of Different Characterization Techniques. *J. Microsc.* **2016**, *264* (1), 88–101.
- (15) Jäsberg, A.; Selenius, P.; Koponen, A. Experimental Results on the Flow Rheology of Fiber-Laden Aqueous Foams. *Colloids Surf., A* **2015**, *473*, 147–155.
- (16) Al-Qararah, A. M.; Ekman, A.; Hjelt, T.; Ketoja, J. A.; Kiiskinen, H.; Koponen, A.; Timonen, J. A Unique Microstructure of the Fiber Networks Deposited from Foam-Fiber Suspensions. *Colloids Surf., A* **2015**, *482*, 544–553.
- (17) Jia, W.; Ren, S.; Hu, B. Effect of Water Chemistry on Zeta Potential of Air Bubbles. *Int. J. Electrochem. Sci.* **2013**, *8*, 5828–5837.
- (18) Bhardwaj, N. K.; Kumar, S.; Bajpai, P. K. Effects of Processing on Zeta Potential and Cationic Demand of Kraft Pulps. *Colloids Surf., A* **2004**, *246* (1–3), 121–125.
- (19) Bhardwaj, N. K.; Hoang, V.; Nguyen, K. L. A Comparative Study of the Effect of Refining on Physical and Electrokinetic Properties of Various Cellulosic Fibres. *Bioresour. Technol.* **2007**, *98* (8), 1647–1654.
- (20) Terpstra, A. S.; Shopsowitz, K. E.; Gregory, C. F.; Manning, A. P.; Michal, C. A.; Hamad, W. Y.; Yang, J.; MacLachlan, M. J. Helium Ion Microscopy: A New Tool for Imaging Novel Mesoporous Silica and Organosilica Materials. *Chem. Commun.* **2013**, *49* (16), 1645–1647.
- (21) Yang, C.; Dabros, T.; Li, D.; Czarniecki, J.; Masliyah, J. H. Measurement of the Zeta Potential of Gas Bubbles in Aqueous Solutions by Microelectrophoresis Method. *J. Colloid Interface Sci.* **2001**, *243* (1), 128–135.
- (22) Stubenrauch, C.; Rojas, O. J.; Schlarmann, J.; Claesson, P. M., II. Interactions between Nonpolar Surfaces Coated with the Nonionic Surfactant Hexaoxyethylene Dodecyl Ether C₁₂E₆ and the Origin of Surface Charges at the Air/Water Interface. *Langmuir* **2004**, *20*, 4977.
- (23) Redlinger-Pohn, J. D.; Grabner, M.; Zauner, P.; Radl, S. Separation of Cellulose Fibres from Pulp Suspension by Froth Flotation Fractionation. *Sep. Purif. Technol.* **2016**, *169*, 304–313.
- (24) Deng, Y. Effect of Fibre Surface Chemistry on the Fiber Loss in Flotation Deinking. *Tappi J.* **2000**, *83*, 1–8.
- (25) Ajersch, M.; Pelton, R. Mechanisms of Pulp Loss in Flotation Deinking. *J. Pulp Pap. Sci.* **1996**, *22* (9), J338–J345.
- (26) Zawala, J.; Karaguzel, C.; Wiertel, A.; Sahbaz, O.; Malysa, K. Kinetics of the Bubble Attachment and Quartz Flotation in Mixed Solutions of Cationic and Non-Ionic Surface-Active Substances. *Colloids Surf., A* **2017**, *523*, 118–126.
- (27) Yang, C.; Dabros, T.; Li, D.; Czarniecki, J.; Masliyah, J. H. A Visualizing Method for Study of Micron Bubble Attachment onto a Solid Surface under Varying Physicochemical Conditions. *Ind. Eng. Chem. Res.* **2000**, *39* (12), 4949–4955.
- (28) Preuss, M.; Butt, H.-J. Direct Measurement of Particle–Bubble Interactions in Aqueous Electrolyte: Dependence on Surfactant. *Langmuir* **1998**, *14* (12), 3164–3174.
- (29) Nguyen, A. V.; Schulze, H. J.; Ralston, J. Elementary Steps in Particle–Bubble Attachment. *Int. J. Miner. Process.* **1997**, *51* (1–4), 183–195.
- (30) Yang, C.; Dabros, T.; Li, D.; Czarniecki, J.; Masliyah, J. H. Analysis of Fine Bubble Attachment onto a Solid Surface within the Framework of Classical DLVO Theory. *J. Colloid Interface Sci.* **1999**, *219* (1), 69–80.
- (31) Ducker, W. A.; Xu, Z.; Israelachvili, J. N. Measurements of Hydrophobic and DLVO Forces in Bubble–Surface Interactions in Aqueous Solutions. *Langmuir* **1994**, *10* (9), 3279–3289.
- (32) Wang, G.; Nguyen, A. V.; Mitra, S.; Joshi, J. B.; Jameson, G. J.; Evans, G. M. A Review of the Mechanisms and Models of Bubble-Particle Detachment in Froth Flotation. *Sep. Purif. Technol.* **2016**, *170*, 155–172.
- (33) Nguyen, A. V.; Ralston, J.; Schulze, H. J. On Modelling of Bubble-Particle Attachment Probability in Flotation. *Int. J. Miner. Process.* **1998**, *53* (4), 225–249.
- (34) Manev, E. D.; Nguyen, A. V. Effects of Surfactant Adsorption and Surface Forces on Thinning and Rupture of Foam Liquid Films. *Int. J. Miner. Process.* **2005**, *77* (1), 1–45.
- (35) Fröberg, J. C.; Rojas, O. J.; Claesson, P. M. Surface Forces and Measuring Techniques. *Int. J. Miner. Process.* **1999**, *56*, 1–30.
- (36) Krasowska, M.; Kolasinska, M.; Warszynski, P.; Malysa, K. Influence of Polyelectrolyte Layers Deposited on Mica Surface on Wetting Film Stability and Bubble Attachment. *J. Phys. Chem. C* **2007**, *111*, 5743.
- (37) Niecikowska, A.; Zawala, J.; Miller, R.; Malysa, K. Dynamic Adsorption Layer Formation and Time of Bubble Attachment to a Mica Surface in Solutions of Cationic Surfactants (CnTABr). *Colloids Surf., A* **2010**, *365* (1–3), 14–20.
- (38) Kor, M.; Korczyk, P. M.; Addai-Mensah, J.; Krasowska, M.; Beattie, D. A. Carboxymethylcellulose Adsorption on Molybdenite: The Effect of Electrolyte Composition on Adsorption, Bubble-Surface Collisions, and Flotation. *Langmuir* **2014**, *30* (40), 11975–11984.
- (39) Kosior, D.; Zawala, J.; Niecikowska, A.; Malysa, K. Influence of Non-Ionic and Ionic Surfactants on Kinetics of the Bubble Attachment to Hydrophilic and Hydrophobic Solids. *Colloids Surf., A* **2015**, *470*, 333–341.
- (40) Wu, J.; Delcheva, I.; Ngothai, Y.; Krasowska, M.; Beattie, D. A. Bubble–Surface Interactions with Graphite in the Presence of Adsorbed Carboxymethylcellulose. *Soft Matter* **2015**, *11* (3), 587–599.
- (41) Krasowska, M.; Kor, M.; Pawlitzak, P.; Bernardis, F. L.; Bradshaw-Hajek, B. H.; Beattie, D. A. Controlling Bubble-Solid Surface Interactions with Environmentally Benign Interfacial Modifiers. *J. Phys. Chem. C* **2019**, *123* (6), 3645–3656.
- (42) Bonn, D.; Eggers, J.; Indekeu, J.; Meunier, J.; Rolley, E. Wetting and Spreading. *Rev. Mod. Phys.* **2009**, *81* (2), 739–805.
- (43) Danov, K. D.; Stanimirova, R. D.; Kralchevsky, P. A.; Marinova, K. G.; Stoyanov, S. D.; Blijdenstein, T. B. J.; Cox, A. R.; Pelan, E. G. Adhesion of Bubbles and Drops to Solid Surfaces, and Anisotropic

Surface Tensions Studied by Capillary Meniscus Dynamometry. *Adv. Colloid Interface Sci.* **2016**, *233*, 223–239.

(44) Baek, Y.; Kang, J.; Theato, P.; Yoon, J. Measuring Hydrophilicity of RO Membranes by Contact Angles via Sessile Drop and Captive Bubble Method: A Comparative Study. *Desalination* **2012**, *303*, 23–28.

(45) Mohammadi, S.; Willers, T. *Development of a Measuring Method for Characterizing the Surface of Pressure Sensitive Adhesives (PSA)*; Kruss: Hamburg, Germany, 2018; Vol. AR287.

(46) Neumann, A. W.; Good, R. J. Techniques of Measuring Contact Angles. In *Surface and Colloid Science*; Good, R. J., Ed.; Plenum Press: New York, 1979; pp 31–91.

(47) Schaub, M.; Wenz, G.; Wegner, G.; Stein, A.; Klemm, D. Ultrathin Films of Cellulose on Silicon Wafers. *Adv. Mater.* **1993**, *5* (12), 919–922.

(48) Wegner, G.; Buchholz, V.; Ödberg, L.; Stemme, S. Regeneration, Derivatization and Utilization of Cellulose in Ultrathin Films. *Adv. Mater.* **1996**, *8* (5), 399–402.

(49) Mohan, T.; Kargl, R.; Doliška, A.; Vesel, A.; Köstler, S.; Ribitsch, V.; Stana-Kleinschek, K. Wettability and Surface Composition of Partly and Fully Regenerated Cellulose Thin Films from Trimethylsilyl Cellulose. *J. Colloid Interface Sci.* **2011**, *358* (2), 604–610.

(50) Kontturi, E.; Thüne, P. C.; Niemantsverdriet, J. W. Cellulose Model Surfaces - Simplified Preparation by Spin Coating and Characterization by X-Ray Photoelectron Spectroscopy, Infrared Spectroscopy, and Atomic Force Microscopy. *Langmuir* **2003**, *19* (14), 5735–5741.

(51) Kontturi, K. S.; Holappa, S.; Kontturi, E.; Johansson, L. S.; Hyvärinen, S.; Peltonen, S.; Laine, J. Arrangements of Cationic Starch of Varying Hydrophobicity on Hydrophilic and Hydrophobic Surfaces. *J. Colloid Interface Sci.* **2009**, *336* (1), 21–29.

(52) Xue, J.; Shi, P.; Zhu, L.; Ding, J.; Chen, Q.; Wang, Q. A Modified Captive Bubble Method for Determining Advancing and Receding Contact Angles. *Appl. Surf. Sci.* **2014**, *296*, 133–139.

(53) Maldonado-Codina, C.; Morgan, P. B. In Vitro Water wettability of Silicone Hydrogel Contact Lenses Determined Using the Sessile Drop and Captive Bubble Techniques. *J. Biomed. Mater. Res., Part A* **2007**, *83A*, 496–502.

(54) Drelich, J.; Miller, J. D.; Good, R. J. The Effect of Drop (Bubble) Size on Advancing and Receding Contact Angles for Heterogeneous and Rough Solid Surfaces as Observed with Sessile-Drop and Captive-Bubble Techniques. *J. Colloid Interface Sci.* **1996**, *179* (1), 37–50.

(55) Lander, L. M.; Siewierski, L. M.; Brittain, W. J.; Vogler, E. A. A Systematic Comparison of Contact Angle Methods. *Langmuir* **1993**, *9* (8), 2237–2239.

(56) Kwok, D. Y.; Neumann, A. W. Contact Angle Measurement and Contact Angle Interpretation. *Adv. Colloid Interface Sci.* **1999**, *81*, 167–249.

(57) Höök, F.; Kasemo, B.; Nylander, T.; Fant, C.; Sott, K.; Elwing, H. Variations in Coupled Water, Viscoelastic Properties, and Film Thickness of a Mefp-1 Protein Film during Adsorption and Cross-Linking: A Quartz Crystal Microbalance with Dissipation Monitoring, Ellipsometry, and Surface Plasmon Resonance Study. *Anal. Chem.* **2001**, *73*, 5796–5804.

(58) Sauerbrey, G. The Use of Quartz Oscillators for Weighing Thin Layers and for Microweighing. *Eur. Phys. J. A* **1959**, *155*, 206–222.

(59) Karlsson, A. P. M.; Palmqvist, A. E. C.; Holmberg, K. Adsorption of Sodium Dodecyl Phosphate and Sodium Dodecyl Sulphate at the Surface of Hydroxyl Aluminium, Studied by QCM-D, XPS and AAS. *Langmuir* **2008**, *24*, 13414–13419.

(60) Johansson, L.-S.; Tammelin, T.; Campbell, J. M.; Setälä, H.; Österberg, M. Experimental Evidence on Medium Driven Cellulose Surface Adaptation Demonstrated Using Nanofibrillated Cellulose. *Soft Matter* **2011**, *7* (22), 10917.

(61) Lindman, B.; Karlström, G.; Stigsson, L. On the Mechanism of Dissolution of Cellulose. *J. Mol. Liq.* **2010**, *156* (1), 76–81.

(62) Naderi, A.; Claesson, P. M. Adsorption Properties of Polyelectrolyte-Surfactant Complexes on Hydrophobic Surfaces Studied by QCM-D. *Langmuir* **2006**, *22* (18), 7639–7645.

(63) Zhang, J.; Meng, Y.; Tian, Y.; Zhang, X. Effect of Concentration and Addition of Ions on the Adsorption of Sodium Dodecyl Sulfate on Stainless Steel Surface in Aqueous Solutions. *Colloids Surf., A* **2015**, *484*, 408–415.

(64) Kronberg, B.; Holmberg, K.; Lindman, B. *Surface Chemistry of Surfactants and Polymers*, 1st ed.; John Wiley & Sons, Inc.: West Sussex, U.K., 2014.

(65) Wanless, E. J.; Ducker, W. A. Organization of Sodium Dodecyl Sulfate at the Graphite - Solution Interface. *J. Phys. Chem.* **1996**, *100*, 3207–3214.

(66) Duan, M.; Wang, H.; Fang, S.; Liang, Y. Real-Time Monitoring the Adsorption of Sodium Dodecyl Sulfate on a Hydrophobic Surface Using Dual Polarization Interferometry. *J. Colloid Interface Sci.* **2014**, *417*, 285–292.

(67) Burgess, I.; Zamlyny, V.; Szymanski, G.; Lipkowski, J.; Majewski, J.; Smith, G.; Satija, S.; Ivkov, R. Electrochemical and Neutron Reflectivity Characterization of Dodecyl Sulfate Adsorption and Aggregation at the Gold–Water Interface. *Langmuir* **2001**, *17* (11), 3355–3367.

(68) Tucker, I. M.; Petkov, J. T.; Penfold, J.; Thomas, R. K. How Electrolyte and Polyelectrolyte Affect the Adsorption of the Anionic Surfactant SDS onto the Surface of a Cellulose Thin Film and the Structure of the Cellulose Film. 1. Hydrophobic Cellulose. *Langmuir* **2012**, *28* (29), 10773–10780.

(69) Rapp, M. V.; Donaldson, S. H.; Gebbie, M. A.; Gizaw, Y.; Koenig, P.; Roiter, Y.; Israelachvili, J. N. Effects of Surfactants and Polyelectrolytes on the Interaction between a Negatively Charged Surface and a Hydrophobic Polymer Surface. *Langmuir* **2015**, *31* (29), 8013–8021.

(70) Nevskaja, D. M.; Guerrero-Ruiz, A.; López-González, J. D. D. Adsorption of Polyoxyethylene Nonionic and Anionic Surfactants from Aqueous Solution: Effects Induced by the Addition of NaCl and CaCl₂. *J. Colloid Interface Sci.* **1998**, *205* (1), 97–105.

(71) Chang, Z.; Chen, X.; Peng, Y. The Adsorption Behavior of Surfactants on Mineral Surfaces in the Presence of Electrolytes – A Critical Review. *Miner. Eng.* **2018**, *121*, 66–76.

(72) Stöckelhuber, K. W. Stability and Rupture of Aqueous Wetting Films. *Eur. Phys. J. E: Soft Matter Biol. Phys.* **2003**, *12* (3), 431–435.

(73) Tucker, I. M.; Petkov, J. T.; Penfold, J.; Thomas, R. K. Interaction of the Anionic Surfactant SDS with a Cellulose Thin Film and the Role of Electrolyte and Polyelectrolyte. 2 Hydrophilic Cellulose. *Langmuir* **2012**, *28* (27), 10223–10229.

(74) Fainerman, V. B.; Lylyk, S. V.; Aksenenko, E. V.; Petkov, J. T.; Yorke, J.; Miller, R. Surface Tension Isotherms, Adsorption Dynamics and Dilational Visco-Elasticity of Sodium Dodecyl Sulphate Solutions. *Colloids Surf., A* **2010**, *354* (1–3), 8–15.

(75) Makkonen, L. A Thermodynamic Model of Contact Angle Hysteresis. *J. Chem. Phys.* **2017**, *147* (6), 064703.

(76) Fuerstenau, D.; Raghavan, S. Some Aspects of Flotation Thermodynamics. In *Froth Flotation: A Century of Innovation*; Fuerstenau, M. C., Jameson, G.; Yoon, R., Eds.; Society for Mining, Metallurgy and Exploration, Inc.: Littleton, CO, 2007; pp 99–111.

(77) Li, Q.; Zhou, P.; Yan, H. J. Pinning-Depinning Mechanism of the Contact Line during Evaporation on Chemically Patterned Surfaces: A Lattice Boltzmann Study. *Langmuir* **2016**, *32*, 9389.

(78) Choi, W.; Tuteja, A.; Mabry, J. M.; Cohen, R. E.; McKinley, G. H. A Modified Cassie-Baxter Relationship to Explain Contact Angle Hysteresis and Anisotropy on Non-Wetting Textured Surfaces. *J. Colloid Interface Sci.* **2009**, *339* (1), 208–216.

(79) Heikkilä, P.; Jetsu, P.; Kinnunen, K.; Määtänen, M.; Valta, K.; Harlin, A. *Sustainable Nonwoven Materials by Foam Forming Using Cellulosic Fibres and Recycled Materials*. 7th Aachen-Dresden International Textile Conference, AD-ITC 2013-Eurogress, Aachen, Germany, 2013.

(80) Ketoja, J. A.; Paunonen, S.; Jetsu, P.; Pääkkönen, E. Compression Strength Mechanisms of Low-Density Fibrous Materials. *Materials* **2019**, *12*, 384.